Rheology of the lithosphere inferred from postseismic uplift following the 1959 Hebgen Lake earthquake

Takuya Nishimura
Geographical Survey Institute, Tsukuba, Ibaraki, Japan

Wayne Thatcher
U.S. Geological Survey, Menlo Park, California, USA

Received 6 September 2002; revised 23 April 2003; accepted 14 May 2003; published 22 August 2003.

[1] We have modeled the broad postseismic uplift measured by geodetic leveling in the epicentral area of the 1959 M_w = 7.3 Hebgen Lake, Montana earthquake, a normal faulting event in the northern Basin and Range province. To fit the observed uplift we calculate synthetic postseismic deformation using the relaxation response of a gravitational viscoelastic Earth to the earthquake. For a model with an elastic plate overlying a viscoelastic half-space, we find that the elastic thickness is 38 ± 8 km, which isclose to the local crustal thickness. The half-space viscosity is estimated at $4 \times 10^{18\pm0.5}$ Pa s. The leveling data do not require a viscous lower crust but permit a lower bound viscosity of 10^{20} Pa s. The observed broad uplift cannot be explained by physically plausible afterslip on and below the coseismic fault. However, local deformation across the coseismic surface rupture requires shallow afterslip reaching the surface. The postseismic deformation induced by the estimated viscoelastic structure decays exponentially with a time constant of ~15 years. Because of coupling between the elastic layer and the viscoelastic substrate, this relaxation time is significantly longer than the 2 year Maxwell relaxation time of the viscous half-space itself. Our result suggests the importance of postseismic relaxation in interpreting high-precision global positioning system velocities. For example, our model results suggest that postseismic transient velocities from both the 1959 Hebgen Lake and the 1983 M_w = 6.9 Borah Peak earthquakes are currently as large as 1–2 mm/yr. *INDEX TERMS:* 1236 Geodesy and Gravity: Rheology of the lithosphere and mantle (8160); 1208 Geodesy and Gravity: Crustal movements—intraplate (8110); 8109 Tectonophysics: Continental tectonics—extensional (0905); *KEYWORDS:* postseismic deformation, viscoelastic relaxation, leveling

Citation: Nishimura, T., and W. Thatcher, Rheology of the lithosphere inferred from postseismic uplift following the 1959 Hebgen Lake earthquake, *J. Geophys. Res.*, *108*(B8), 2389, doi:10.1029/2002JB002191, 2003.

1. Introduction

[2] Deformation of the Earth is strongly influenced by its rheological layering. On the continents it is widely accepted that the upper crust is brittle and elastic, and the mantle deforms by ductile flow. However, the thickness of the elastic part of the crust, the rheological behavior of the lower crust, and the viscosity structure of the upper mantle are not yet well constrained and appear to vary widely.

[3] Transient crustal deformation induced by large crustal earthquakes has been used to infer the rheology of the continental crust and upper mantle [e.g., *Thatcher et al.*, 1980; *Tabei*, 1989; *Deng et al.*, 1998; *Pollitz et al.*, 1998, 2000, 2001]. These studies suggest that the elastically strong part of the lithosphere is thin (~10–30 km) and the underlying substratum has a low viscosity (10^{17}–10^{20} Pa s). Inferences based on reservoir loading [*Kaufmann and Amelung*, 2000] and isostatic rebound from draining of pluvial lakes [e.g., *Iwasaki and Matsu'ura*, 1982; *Nakiboglu and Lambeck*, 1983; *Bills and May*, 1987; *Bills et al.*, 1994] give values within the same range. In contrast, postglacial rebound studies in the stable Fennoscandian and Canadian Shields [e.g., *Lambeck et al.*, 1998; *Milne et al.*, 2001] generally indicate elastic plate thickness of ~100 km overlying a high-viscosity substratum (>10^{20} Pa s). The considerable variability among these results, even in actively deforming regions, suggests the value of additional well-documented case studies. Here we examine deformation following the 1959 M_w = 7.3 Hebgen Lake, Montana earthquake to estimate the local rheological layering.

[4] The Hebgen Lake earthquake of 17 August 1959 is one of the largest historical earthquakes to have occurred in the Basin and Range province [*Smith and Arabasz*, 1991]. The epicenter locates ~20 km northwest of the Yellowstone caldera where active volcanic and hydrothermal activity occurs. Surface fault slip locally exceeded 6 m and dip-slip motions inferred to occur at depth were in the range 7–10 m

0148-0227/03/2002JB002191$09.00

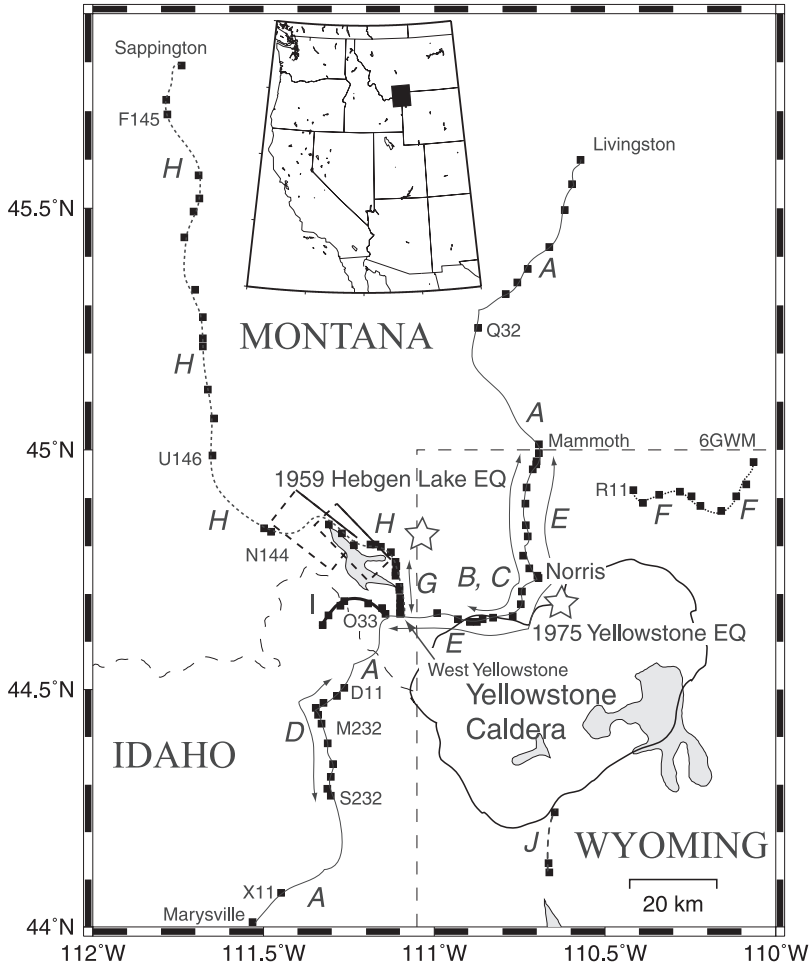

Figure 1. Location of leveling routes in the Yellowstone-Hebgen Lake region and regional scale map (inset). Lines along benchmarks indicated by solid squares are leveling routes used in this study. Italic letters (*A*-*J*) name the data subsets listed in Table 1. Several leveling segments such as *B*, *C*, *D*, *E*, and *G* are part of longer leveling routes indicated by the double arrowed lines. Thin dashed line is State boundary. Two stars are the epicenters of the 1959 Hebgen Lake and the 1975 Yellowstone earthquakes [*Smith and Arabasz*, 1991]. Rectangles show the two fault planes of the Hebgen Lake earthquake [*Barrientos et al.*, 1987] with the upper edge indicated by a solid line.

[*Barrientos et al.*, 1987]. *Reilinger* [1986] first noted the distinctive transient uplift following the earthquake and pointed out that it could be explained by viscoelastic relaxation in a subcrustal layer. Based on examination of a single leveling route and using modeling results from *Thatcher et al.* [1980], he suggested a model with a 30–40 km thick elastic layer overlying a viscoelastic half-space with a viscosity of $\sim 10^{19}$ Pa s. *Holdahl and Dzurisin* [1991] clarified the space-time deformation by interpolating repeated leveling surveys carried out from 1923 to 1987 in the Hebgen Lake-Yellowstone region. Their results clearly show the broad spatial extent and large amplitude of the postseismic uplift, which extends more than 80 km from the 1959 epicenter and locally exceeds 300 mm.

[5] In this paper, we reexamine the 1959–1987 leveling data from the epicentral area of the 1959 Hebgen Lake and use it to constrain the rheological structure of the crust and upper mantle. Based on our derived rheology profile we estimate the postseismic effects of two other large twentieth century Basin and Range earthquakes and assess their influence on the current (2002) global positioning system (GPS) velocity field.

2. Data and Method

2.1. Leveling Data

[6] Figure 1 shows the leveling routes used in this study. The benchmarks were leveled to first-order leveling standards along a number of segments following the 1959 earthquake. *Holdahl and Dzurisin* [1991] describe the space-time sequence of the deformation in detail. In the Yellowstone caldera, distinct uplift and subsidence events have been observed from both leveling [*Holdahl and Dzurisin*, 1991; *Dzurisin et al.*, 1994] and InSAR measurements [*Wicks et al.*, 1998]. These movements are associated with volcanic activity within Yellowstone caldera, and we exclude them from our analysis.

[7] We modeled the relative elevation change in each section between adjacent benchmarks rather than the cumulative elevation changes along a leveling route, which

Table 1. Data Subset Used in This Study

	First Survey		Second Survey		
Data Subset	NGS Number	Year	NGS Number	Year	Number of Section
A	L18004, L18098, L18101	1960.6–7	L24756	1983.6	15
B	L18098	1960.7	L25091/4	1975.6	15
C	L25091/4	1975.6	L24756	1983.6	15
D	L18004	1960.6	L21139	1967.6	10
E	L24756	1983.6	L25059/6, L25059/7	1987.5–7	21
F	L25091/7	1977.6	L25059/1, L25059/8	1987.6–7	9
G	L17565	1959.8	L18104	1960.6	7
H	L17565	1959.8	L25059/1	1987.6	25
I	L19913	1964.7	L24756	1983.6	6
J	L25091/5	1977.5	L25059/2	1987.7	2
K	L18098	1960.7	L25091/3	1976.7	2
M	L25091/3	1976.7	L24756	1983.6	2
N	L18104	1960.6	L25059/1	1987.6	2

requires knowing or assuming the change in elevation of a reference benchmark. Our approach has the advantage that the relative elevation change in each section is a direct measurement and we avoid any dependence of modeling results on the reference benchmark. The total number of data is 131 and the data are grouped into 13 subsets listed in Table 1. In each subset named A-N, the data are relative elevation changes in the same time interval. We plot routes of 10 subsets denoted as A-J in Figure 1. The other three subsets, K-N in Table 1, have only two measurements and their routes overlap route A and H.

[8] Leveling errors can be random or systematic. Systematic errors are caused by inappropriate corrections for the atmospheric refraction and rod thermal expansion. They tend to be correlated with elevation of benchmarks. Because the observed deformation is not systematically correlated with topography [*Holdahl and Dzurisin*, 1991], we neglect the systematic errors. Random error s of elevation difference in a section between two benchmarks is given by $s = a\sqrt{L}$, where s is in mm, a is a constant factor, and L is distance in km. Here a is 1.0 mm/$\sqrt{\text{km}}$ for surveys before 1977 and 1.4 mm/$\sqrt{\text{km}}$ for the survey after 1983 [*Holdahl and Dzurisin*, 1991]. The uncertainty σ_i of changes of elevation difference in the ith section is given by

$$\sigma_i = \sqrt{\alpha^2 L_i + \beta^2}, \tag{1}$$

where $\alpha = \sqrt{a_1^2 + a_2^2}$ with a_1 and a_2 corresponding to the values of a for two surveys, and L_i is length of the ith section in km. Following *Kaufmann and Amelung* [2000], we introduced an additional uncertainty β to account for unmodeled deformation from local earthquakes, fault movements, and other causes. In section 3.1, we discuss and model one such deformation source detected in the leveling data. Introduction of the factor β permits us to decrease the data weight in specified sections and improve the fit of our preferred model to the data. By trial and error testing, we adopted a value for β of 2 mm.

2.2. Postseismic Model of the Hebgen Lake Earthquake

[9] To calculate the viscoelastic postseismic deformation we adopt the two-plane earthquake fault model of *Barrientos et al.* [1987] estimated from inversion of coseismic leveling data and lake shoreline changes. The model consists of two rectangular fault planes on which pure normal slip of 7.8 and 7.0 m occurred. The locations of the faults are shown in Figure 1. Assuming an elastic shear modulus of 30 GPa, the cumulative seismic moment for the two-fault model is 1.2×10^{20} N m (M_w7.3). We calculate postseismic deformation by using the FORTRAN code VISCO1D [*Pollitz*, 1997], which calculates postseismic deformation due to viscoelastic relaxation of a layered spherical Earth, and includes the effects of gravity and medium compressibility.

2.3. Parameter Search of Viscoelastic Structure

[10] We use a forward modeling procedure to estimate parameters of viscoelastic structure that is in accord with the data. We calculate postseismic displacement in each section between two benchmarks varying parameters within a specified range, and calculate a χ^2 function between observed and calculated displacement for each set of parameters. The χ^2 function is described in vector form as follows:

$$\chi^2 = [\mathbf{d} - \mathbf{p}]^T \mathbf{C}^{-1} [\mathbf{d} - \mathbf{p}], \tag{2}$$

where $\mathbf{d}$ is the observation, $\mathbf{p}$ is the model prediction, and $\mathbf{C}$ is the data covariance matrix. An observed displacement of a leveling section has a small correlation with that of the adjacent section because two adjacent sections share one benchmark. Here we neglect the correlation between them and use $C_{ij} = \delta_{ij}\sigma_i$ as the data covariance matrix. The root-mean-square (rms) misfit is given by

$$\text{rms} = \sqrt{\frac{\chi^2}{n}}, \tag{3}$$

where n is number of data. The rms misfit does not express the range of model parameters which satisfy the observations within their uncertainties. In order to clarify parameter uncertainties, we introduce the statistic γ [*Lambeck et al.*, 1998] as:

$$\gamma^2 = \frac{1}{n} [\hat{\mathbf{p}} - \mathbf{p}]^T \mathbf{C}^{-1} [\hat{\mathbf{p}} - \mathbf{p}], \tag{4}$$

where $\hat{\mathbf{p}}$ is the model prediction whose parameters minimize the rms misfit. The statistic γ has a χ^2 distribution with $n -$

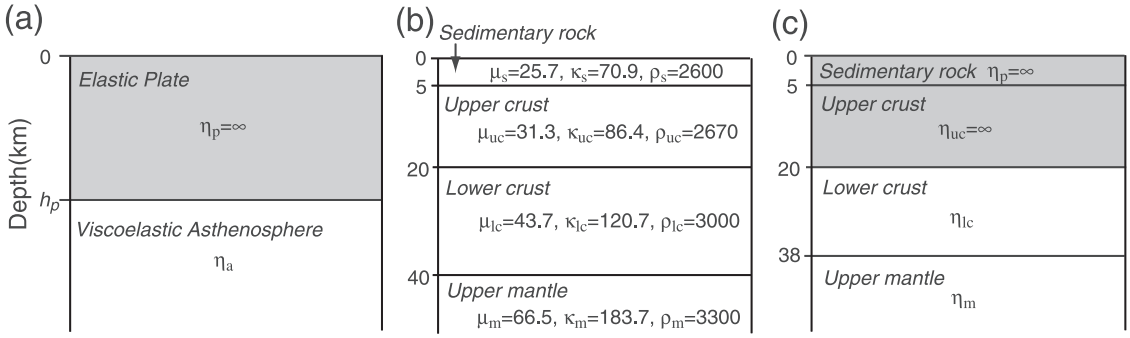

Figure 2. Elastic modulus and viscosity of the layered Earth models. Gray layers are purely elastic. (a) Viscosity and depth of layers of the VE-1 model (see text). (b) Shear modulus (μ), bulk modulus (κ), and density (ρ) in unit of GPa, GPa, and kg/m^3 of the VE-1 model. (c) Viscosity and depth of layers of the VE-2 model (see text).

4 degrees of freedom and models with $n\gamma^2 \leq \chi^2|_{n-4,\zeta}$ satisfy the observations at the ζ confidence limit. We estimate the uncertainty of model parameters from models with $\gamma^2 \leq 1$. We therefore obtain uncertainties for the best fitting model that directly reflect the data uncertainties [*Lambeck et al.*, 1998].

3. Results and Discussion

3.1. Elastic Plate and Viscoelastic Asthenosphere

[11] Here we consider a simple Earth model consisting of an elastic plate overlying a viscoelastic half-space as shown in Figure 2a. The model parameters are the thickness h_p of the elastic plate and the viscosity η_a of the viscoelastic half-space. We varied the parameters h_p and η_a in the range of 20–70 km and 10^{16}–10^{21} Pa s. Intervals of the parameter search for h_p and log η_a are 2 km and 0.1, respectively. We assumed a model of elastic modulus variation with depth based on the seismic *P* wave velocity structure of the region [*Peng and Humphreys*, 1998]. The parameters of this structure are shown in Figure 2b. We refer to this viscoelastic Earth model as the VE-1 model.

[12] Figure 3 shows the rms misfit in model parameter space. The minimum value of the rms misfit is 4.97 at h_p = 38 km and $\eta_a \sim 4 \times 10^{18}$ Pa s. The gray area in Figure 3 identifies the uncertainties of the model parameters. It suggests that models with $h_p = 38 \pm 8$ km and $\eta_a \sim 4 \times 10^{18\pm0.5}$ Pa s satisfy the leveling data as well as the preferred model given the data uncertainties. If the data are perfectly modeled by viscoelastic relaxation of the VE-1 model within their uncertainties, the rms misfit is expected to be 1. However, the minimum rms misfit of 4.97 indicates that the calculated displacements do not fit the observed ones within their uncertainties. This suggests that not all of the observed deformation is due to viscoelastic relaxation, a matter we will discuss further below and in section 3.4.

[13] Figure 4 shows the vertical displacement calculated by the best fitting model for each leveling section. We plotted 123 sections of data subset A, B,. . ., I out of the total 131 sections. The observed and calculated displacements are small except for subsets A and H. Some of the larger misfits are easily explained. First, there is a local disturbance near Norris in Figure 4b. We think that this deformation is associated with the 1975 *M*6.1 Yellowstone earthquake because the epicenter is located ~10 km east of the leveling route (Figure 1). We also see a large discrepancy between the observed and calculated displacements around 20 km in Figure 4h. The sections having large misfits locate across the coseismic surface rupture of the 1959 Hebgen Lake earthquake. In section 3.4, we explain this signal by shallow afterslip. There are also large misfits around 40 and 60 km in Figure 4h. Because the sum of observed displacement over three sections from 31 to 74 km is roughly equal to that of the calculated one, we believe that the misfits can be explained by local deformation near benchmark N144.

[14] The cumulative displacement along the leveling routes, which shows broad uplift in the epicentral area, is explained by the calculated cumulative displacement of VE-1 model. However, the relative uplift of 150 mm during 1960–1983 at Livingstone, on the northeastern end of

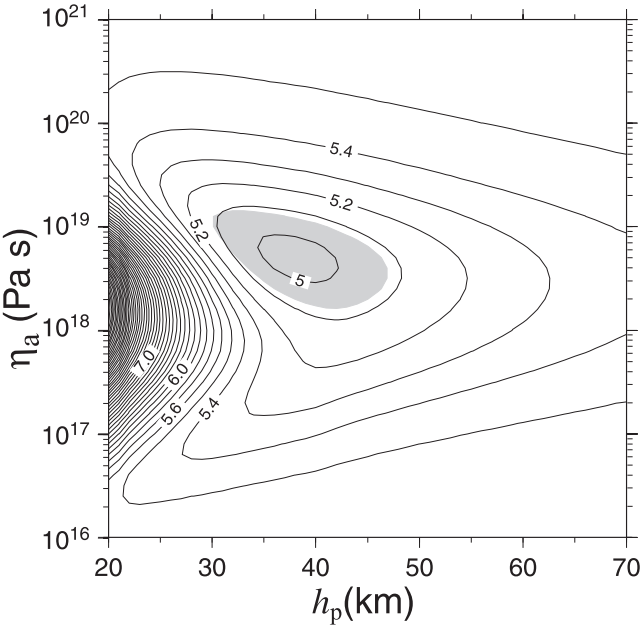

Figure 3. The rms misfit between the calculated and the observed displacements as a function of elastic plate thickness (h_p) and asthenosphere viscosity (η_a) for the VE-1 model. The gray area represents model parameters with statistic $\gamma^2 < 1$.

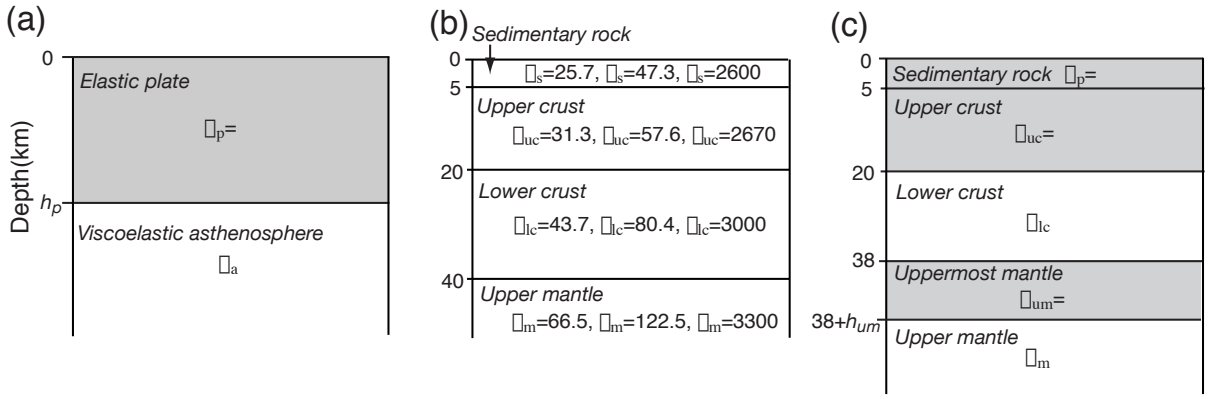

Figure 2. Figure 2 in the original paper is incorrect. This is the correct one and the correction will be published soon!

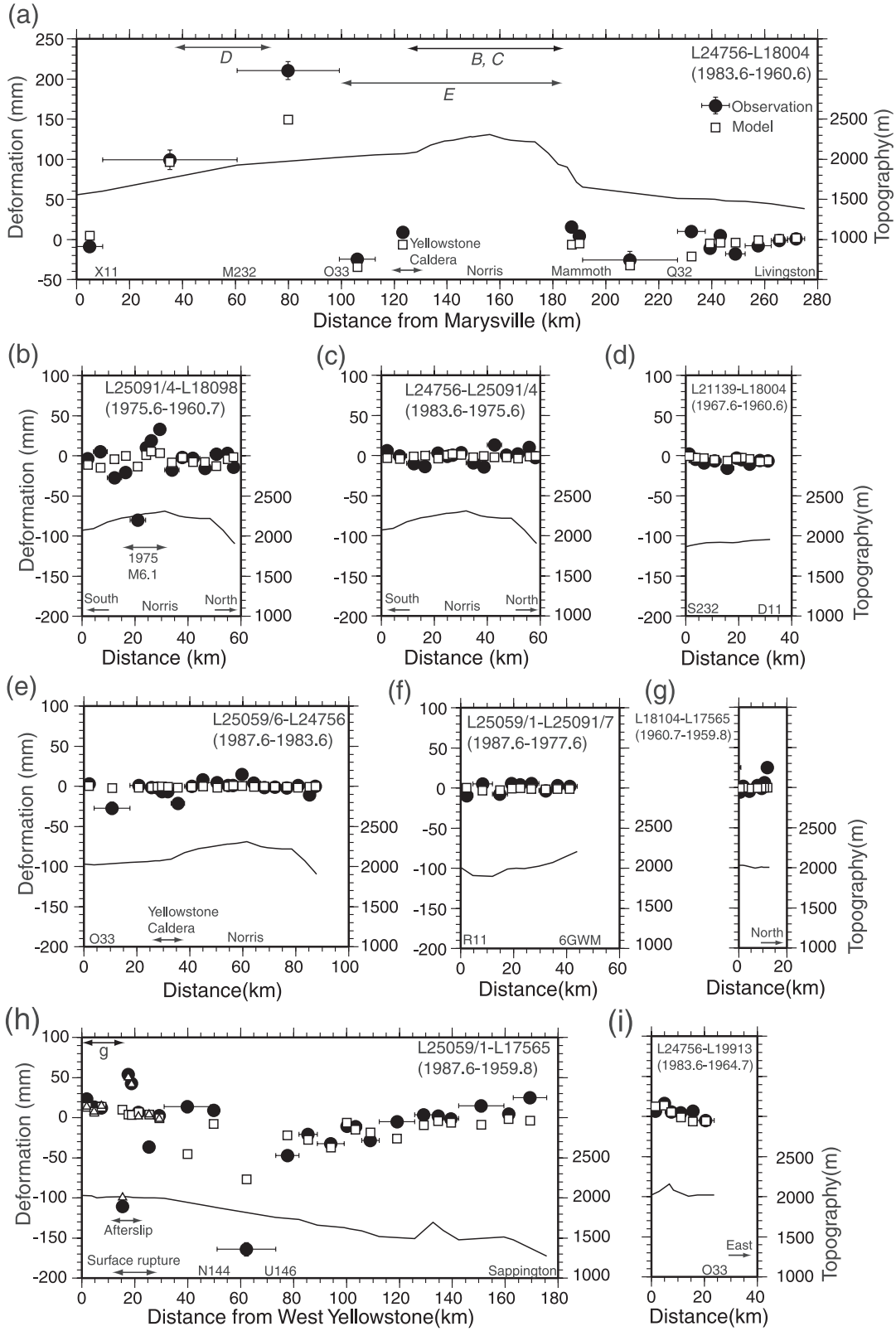

Figure 4. Observed (solid circles) and calculated (open squares) displacements of each section along the leveling routes. Profiles of topography along the leveling routes are indicated by thin solid lines. Horizontal and vertical error bars are ranges of sections and measurement uncertainties, respectively. (a–h) Correspond to data subsets A-H, respectively. The NGS number and year of leveling surveys are indicated. Leveling routes overlapping other routes are indicated in Figures 4a and 4h. The local displacements identified in Figure 4b may be associated with the 1975 *M*6.1 Yellowstone earthquake. Open triangles shown in Figure 4h are displacements calculated by the shallow afterslip model (see text).

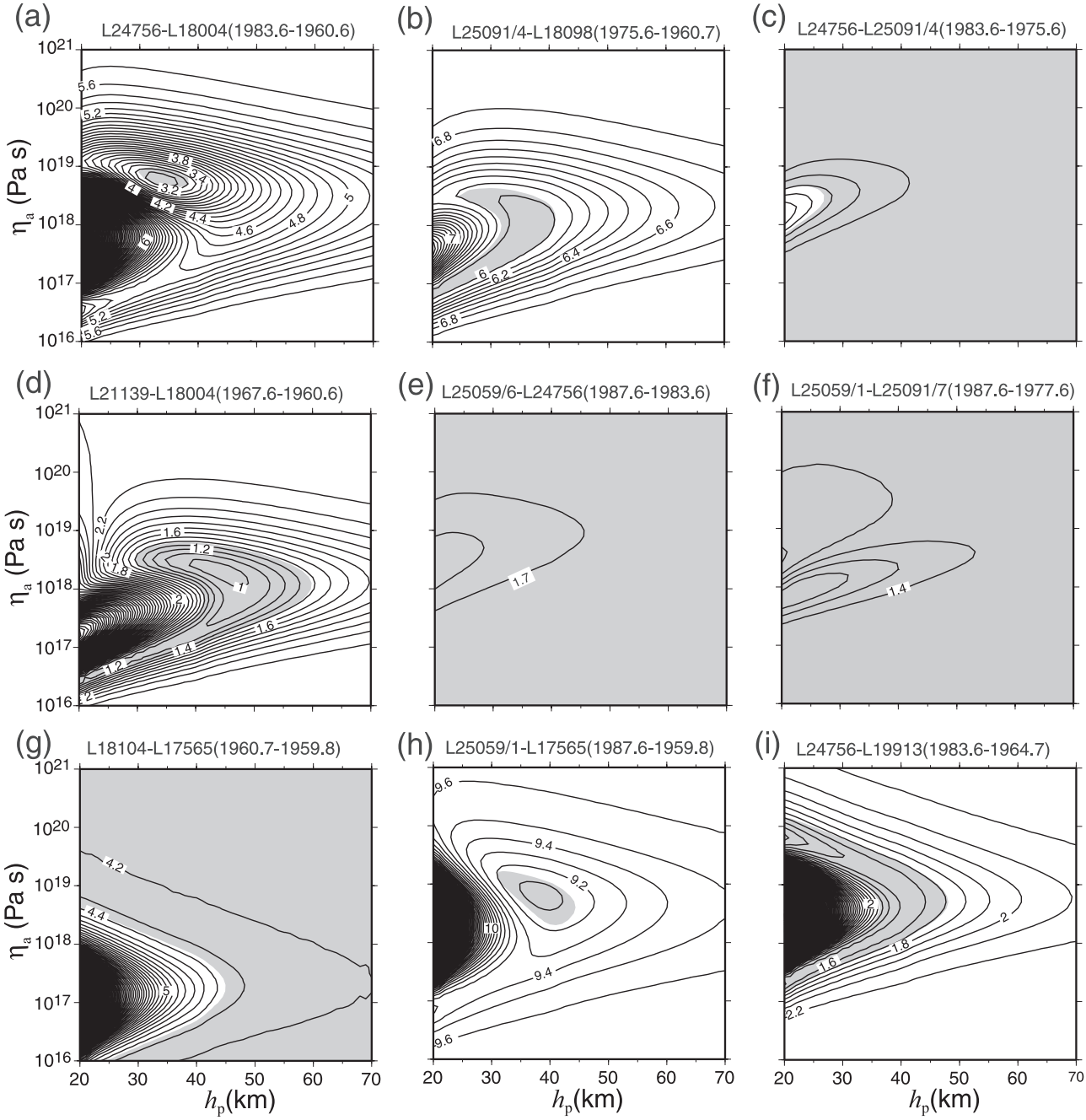

Figure 5. The rms misfit between the calculated and the observed displacements for each subset of the leveling data as a function of elastic plate thickness (h_p) and asthenosphere viscosity (η_a) for the VE-1 model. The gray area represents model parameters with statistic $\gamma^2 < 1$. The NGS number and year of each subset of the leveling data are indicated.

leveling route A (see Figure 1) was observed with respect to Marysville at the southwestern end of route A. The calculated displacement for VE-1 model is roughly the same at both ends of route A and does not explain the observed 150 mm offset between Marysville and Livingstone. We suspect that the leveling survey accomplished in 1960 may have a large-scale systematic error. We base this suspicion on the observed 1923–1960 subsidence of 100 mm at Livingstone with respect to Marysville. Since the magnitude of this large-scale subsidence is close to the observed 1960–1983 large-scale uplift between these points, we suspect a long-wavelength error in the 1960 survey.

[15] We checked the consistency of each data subset by calculating individual rms misfits as shown in Figure 5. The gray areas indicate the uncertainties with respect to the best fitting models in each subset. Only two data sets (A and H), shown in Figures 5a and 5h, constrain the model parameters well. The data used in the previous study of the postseismic deformation of the Hebgen Lake earthquake [*Reilinger*, 1986] correspond to our data subset A. The parameters

satisfying subset A are h_p = 34 ± 4 km and $\eta_a \sim 5 \times 10^{18\pm0.2}$ Pa s. These values are consistent with Reilinger's estimate of h_p = 30–40 km and $\eta_a \sim 10^{19}$ Pa s. In our analysis, the usage of all of the available data did not reduce the uncertainties of the estimated parameters because some of these additional data are affected by shallow afterslip and/or have very small signal-to-noise ratio. Though the parameters minimizing the misfits differ for each subset, the values h_p = 38 km and $\eta_a \sim 4 \times 10^{18}$ Pa s satisfy all data subsets within the uncertainties.

[16] The estimated thickness of the elastic plate (38 ± 8 km) is approximately equal to the local crustal thickness. Seismological studies suggest that the crustal thickness is ~42 km in the eastern Snake River Plain, ~100 km southwest of the Hebgen Lake region [*Braile et al.*, 1982] and that it shallows to ~37 km in the surrounding mountain area [*Peng and Humphreys*, 1998]. This concordance suggests that the elastic plate and the viscoelastic half-space of the VE-1 model are identified as the crust and the upper mantle, respectively.

3.2. Weak Lower Crust and Strong Uppermost Mantle

[17] The result of the previous section suggests that the whole crust including the lower crust is elastic and that the upper mantle has low viscosity. However, studies of post-seismic deformation [*Deng et al.*, 1998; *Pollitz et al.*, 1998] suggest that the lower crust is weak and has low viscosity. Occurrence of earthquakes in uppermost mantle [e.g., *Chen and Molnar*, 1983] suggests that the uppermost mantle is strong and has high viscosity. Laboratory experiments [e.g., *Kohlstedt et al.*, 1995] support the weak lower crust and strong uppermost mantle, if the lower crust and the upper mantle are wet and dry, respectively, under the usual thermal regime. Many scientists have favored the idea that the continental lithosphere generally consists of the weak lower crust sandwiched between the relatively strong upper crust and uppermost mantle.

[18] Here we examine the viscoelastic lower crust and an elastic layer at the top of the upper mantle. We estimate the viscosity of the lower crust as well as that of the upper mantle to constrain the bounds on the lower crustal viscosity, consistent with our data. We also estimate thickness of the pure elastic uppermost mantle, denoted as $h_{\rm um}$. We fixed the thickness of the crust to 38 km, as found in the previous section. We divided the crust into an upper sedimentary layer 5 km thick, an upper crustal layer of 15 km, and an 18 km thick lower crust. Elastic moduli of each layer are as in Figure 2b but the crust-mantle boundary is 38 km instead of 40 km. The sedimentary layer, the upper crust, and the uppermost mantle are assumed to be purely elastic. The lower crust and the upper mantle have viscosities denoted as $\eta_{\rm lc}$ and η_m, respectively. The viscosity structure is diagrammed in Figure 2c and is referred to as the VE-2 model. The ratio of lower crust to upper mantle viscosity ($\eta_{\rm lc}/\eta_m$), the mantle viscosity (η_m), and the thickness of the elastic uppermost mantle ($h_{\rm um}$) are free parameters in the model search. The range of the parameter search for $\eta_{\rm lc}/\eta_m$, η_m, and $h_{\rm um}$ is 10^{-1}–10^4, 10^{16}–10^{21} Pa s, and 0–100 km, respectively. We calculated the synthetic displacements at intervals of 0.2, 0.1, and 10 km for $\log(\eta_{\rm lc}/\eta_m)$, $\log \eta_m$, and $h_{\rm um}$. None of the models in the search space has rms misfit less than that of the best fitting VE-1 model ($\eta_{\rm lc}/\eta_m = \infty$, $\eta_m \sim 4 \times 10^{18}$ Pa s, and $h_{\rm um}$ = 0 km). Figure 6a shows the rms misfit as a function of $\eta_{\rm lc}/\eta_m$ and $h_{\rm um}$. The mantle viscosity is fixed to be $\sim 4 \times 10^{18}$ Pa s in the plot. The minimum rms misfit of 4.97 is found at $\eta_{\rm lc}/\eta_m \geq 300$ and

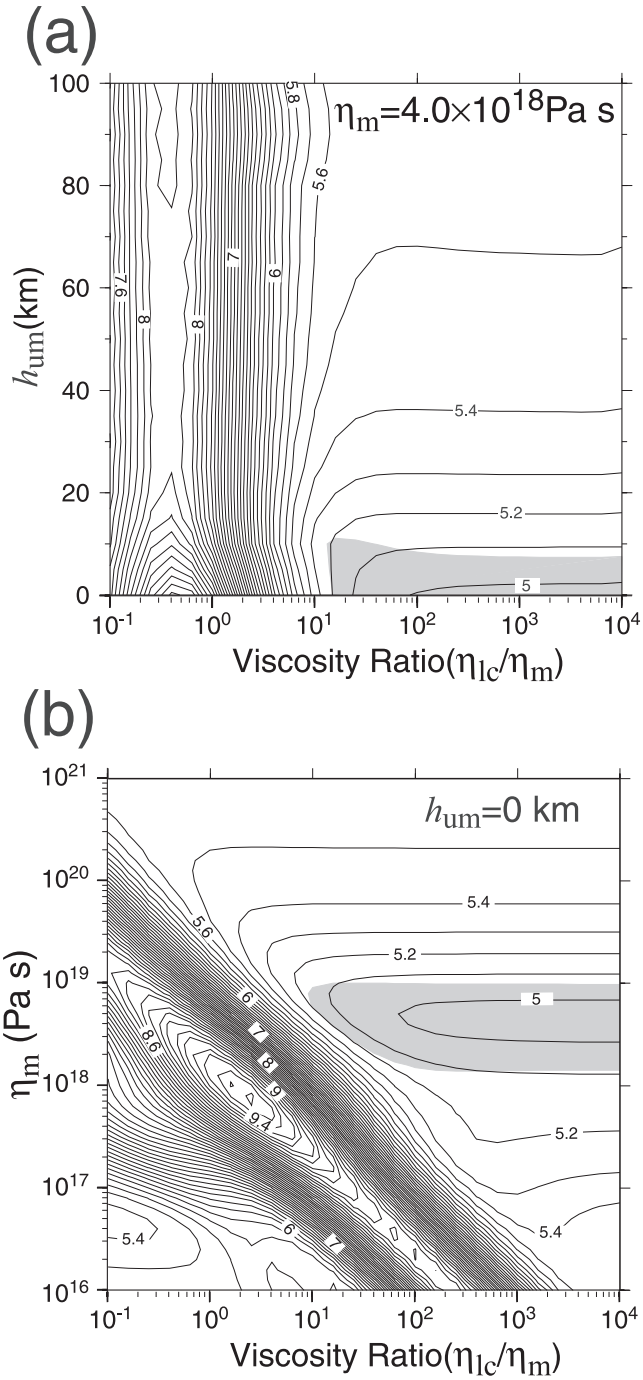

Figure 6. The rms misfit between the calculated and the observed displacements for the VE-2 model. The gray area represents model parameters with statistic $\gamma^2 < 1$. (a) The rms misfit as a function of thickness of the elastic uppermost mantle ($h_{\rm um}$) and lower crust-to-mantle viscosity ratio ($\eta_{\rm lc}/\eta_m$). The viscosity of the upper mantle is fixed to be ~4 × 10^{18} Pa s. (b) The rms misfit as a function of mantle viscosity (η_m) and lower crust-to-mantle viscosity ratio ($\eta_{\rm lc}/\eta_m$) without the elastic uppermost mantle ($h_{\rm um}$ = 0 km).

$h_{um} = 0$ km. The rms misfit increases rapidly as the thickness of the elastic uppermost mantle increases. When the thickness of the elastic uppermost mantle (h_{um}) is fixed to be 0 km, we find the minimum rms misfit of 4.97 at $\eta_{lc}/\eta_m \geq 300$ and $\eta_m \sim 4 \times 10^{18}$ Pa s in Figure 6b. The gray area in Figures 6a and 6b defines the uncertainties of parameters with respect to the best fitting VE-1 model. Though the model with elastic lower crust and no elastic uppermost mantle is the best model to reproduce the observed deformation, the models with $\eta_{lc}/\eta_m \geq 10$, $\eta_m \sim 4 \times 10^{18\pm0.5}$ Pa s, and $h_{um} \leq 10$ km can satisfy the leveling equally well. The leveling data in the Hebgen Lake region thus do not require any mobility of the lower crust and a strong layer of the uppermost mantle, but permit lower crustal viscosities $>10^{20}$ Pa s and thickness of the elastic uppermost mantle $\leq$10 km.

3.3. Comparison With Other Results

[19] Our results are broadly consistent with other studies inferring lithospheric rheology in the Basin and Range province. Lake Bonneville was a late Pleistocene lake 400 km south of the Hebgen Lake region, where the crust rebounded and uplifted due to sudden removal of the lake load 12 to 14 ka B.P. Several authors studied the deformed shorelines of Lake Bonneville to estimate rheological structure. Studies using a simple Earth model like our VE-1 model find that the elastic lithosphere is 23–40 km thick and the asthenosphere viscosity is 1.5×10^{19}–2×10^{20} Pa s [*Iwasaki and Matsu'ura*, 1982; *Nakiboglu and Lambeck*, 1983; *Bills and May*, 1987]. *Bills et al.* [1994] apply a model that permits an arbitrary number of viscoelastic layers and suggest a viscosity of 2×10^{24} Pa s in the top 10 km, $\sim 10^{21}$ Pa s from 10 to 40 km, 4×10^{17}–5×10^{18} Pa s from 40 to 150 km, and higher viscosities at greater depths. However, their simplest model, analogous to our VE-1 model, has an elastic lithosphere 25 km thick, an underlying viscosity of 1.8×10^{19} Pa s, and fits their data nearly as well as the more complex multilayered viscosity model.

[20] *Kaufmann and Amelung* [2000] have used the time-dependent subsidence following reservoir impoundment to infer lithospheric rheology in the southeastern Basin and Range province. Lake Mead, located about 1000 km south of Hebgen Lake, is a large artificial reservoir formed by the construction of the Hoover Dam. Kaufmann and Amelung show that postimpoundment leveling data are consistent with two models. The simplest, like VE-1, has an elastic crust whose thickness is 30 ± 3 km and an underlying half-space with a viscosity of $10^{18\pm0.2}$ Pa s. A second model has the same half-space viscosity but subdivides the crust into a 10 km thick elastic upper layer and a 20 km thick viscoelastic lower crust with a lower bound viscosity of 10^{20} Pa s.

[21] In summary, our results and those cited above have several consistent features. First, in the simplest models, the entire crust is elastic and the upper mantle viscosity lies in the range 10^{18}–10^{20} Pa s. Second, a lower crustal viscosity of at least 10^{20} Pa s is permitted by the data but is not required. Low viscosity of the uppermost mantle in the Basin and Range province may imply its very high temperature according to laboratory experiments of dry olivine flow [e.g., *Pollitz et al.*, 2000]. The presence of water can also drastically reduce the ductile strength of olivines [e.g., *Kohlstedt et al.*, 1995]. *Jackson* [2002] suggests that the upper mantle beneath the continents is relatively weak in most region of the world because of a wet upper mantle. We speculate that the estimated low viscosity is attributed to the presence of water in the uppermost mantle.

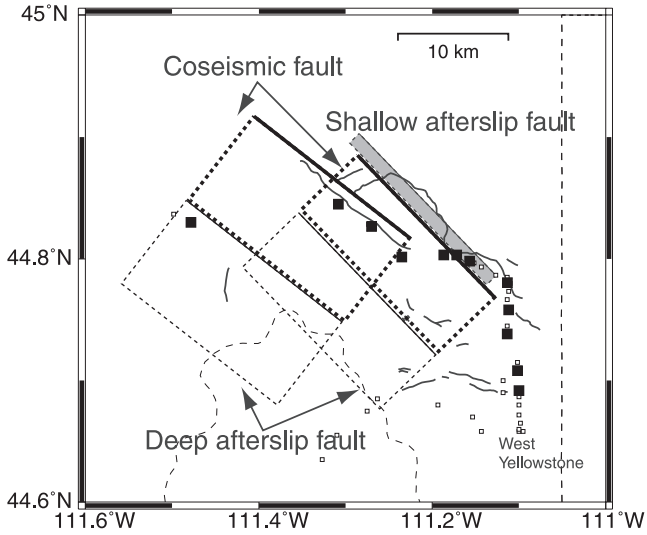

Figure 7. Location of the shallow postseismic afterslip model (shaded rectangle). Thick large rectangles indicate the 1959 earthquake fault planes. The solid lines on the rectangles show their upper edges. The coseismic faults are from the work of *Barrientos et al.* [1987]. Surface ruptures of the 1959 earthquake are indicated by thick solid lines. Benchmarks indicated by solid squares are used to construct the afterslip model.

3.4. Evidence of Shallow Afterslip

[22] The short wavelength deformation in the 10–30 km distance range of Figure 4h cannot be explained by our viscoelastic model. This deformation is characterized by distinctive subsidence on the hanging wall side of the surface trace of the coseismic rupture and is similar to the coseismic displacement pattern. Shallow afterslip in the same sense as the coseismic faulting is thus the likeliest cause of the deformation. Since it is difficult to uniquely estimate fault parameters from the sparse data, we constrain some of them and invert for the remaining ones. We assumed that the postseismic fault reached the surface and its strike, dip, and rake were the same as those of the southeastern coseismic fault segment of *Barrientos et al.* [1987]. The input data are the residuals between the observed displacement and the displacement calculated from the best fitting VE-1 model. We inverted these residual displacements on nine leveling sections to estimate horizontal location, fault width, and slip using the nonlinear inversion algorithm of *Matsu'ura and Hasegawa* [1987]. Synthetic displacements were calculated for slip on a rectangular fault segment in a homogeneous elastic half-space [*Okada*, 1985].

[23] Figure 7 shows the location of the shallow afterslip fault obtained in the inversion. It is located 2 km northeast of the southeast coseismic fault and has 0.25 m of normal slip. The fault width is estimated to be 1.7 km, which means that the depth of the lower edge of the fault is 1.2 km. The upper depth of the southeastern coseismic fault is 1.7 km. The geometry of the postseismic and the coseismic faults thus suggests that afterslip occurred on the shallow

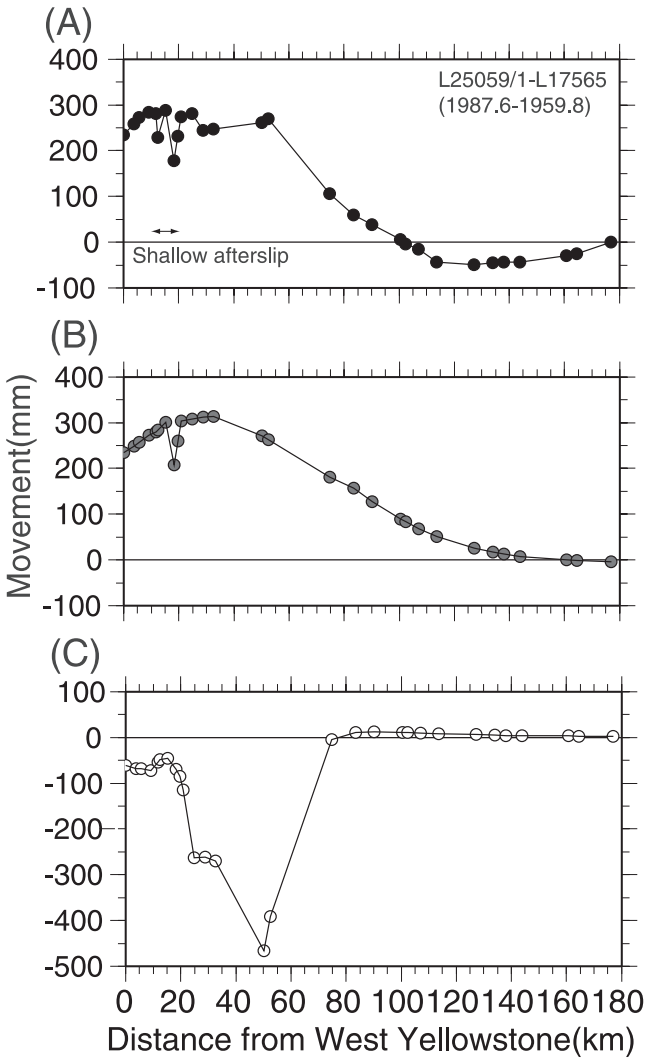

Figure 8. Comparison of cumulative elevation changes along the leveling route A with respect to Marysville. (a) Observed displacements from 1960 to 1983. (b) Synthetic displacements calculated by the best fitting VE-1 model and the shallow afterslip model. (c) Synthetic displacements calculated by the hypothetical deep afterslip on the downdip of the coseismic fault.

extension of the coseismic fault rupture. The vertical displacements calculated by the afterslip model are shown in Figure 4h. The model matches the observed displacements reasonably well. A discrepancy at 25 km, near the coseismic surface rupture, suggests complexity that cannot be explained by our simple one segment model. The shallow afterslip model decreases the total rms misfit from 4.97 to 3.48. The seismic moment of the shallow afterslip estimated above is 2.0×10^{17} N m (M_w5.5), about three orders of magnitude smaller than the coseismic moment of 1.2×10^{20} N m. We note that the leveling survey across the faults was accomplished 1 month after the Hebgen Lake earthquake. Thus any afterslip occurring within a month after the earthquake would be included in the coseismic model.

[24] Afterslip occurring on the coseismic fault or its deeper extension, as has been inferred after other earthquakes [e.g., *Pollitz et al.*, 1998; *Nishimura et al.*, 2000; *Bürgmann et al.*, 2002], cannot explain the post Hebgen Lake earthquake deformation. We show an example of synthetic deformation calculated by hypothetical afterslip on downdip extension of the coseismic fault in Figure 8. We assumed the same fault parameters of the deep afterslip as those of the coseismic fault except that slip magnitude was one third of the coseismic slip and the fault segments lie on the deep extension of the coseismic fault, as shown in Figure 7. The calculated deformation (Figure 8c) cannot apparently explain the observed deformation (Figure 8a). Although the observed displacements are characterized by broad uplift, the deep afterslip requires sharp subsidence near the afterslip fault. We found that applying such an afterslip model we could match the data as well as the VE-1 model only by assuming reverse slip on a rectangular fault segment below about 40 km depth. We rejected this physically unreasonable model and conclude that viscoelastic relaxation is the preferred mechanism of postseismic deformation at Hebgen Lake.

3.5. Horizontal Deformation

[25] *Savage et al.* [1993] studied horizontal deformation of a 40 km aperture trilateration network centered on the 1959 Hebgen Lake earthquake that was surveyed between 1973 and 1987. The data are matched well by a uniaxial N15° ± 1°E extension at a rate of 0.266 ± 0.014 μstrain/yr. The extension is normal to the Hebgen Lake fault and the rate is surprisingly high (comparable to shear strain rates on the San Andreas fault in California), suggesting that it may be a residual effect of the 1959 earthquake. To test this possibility we compare the deformation expected from our best fitting viscoelastic relaxation model VE-1 with the trilateration observations. Observed and computed velocities for the interval 1973–1987 are shown in Figure 9. In

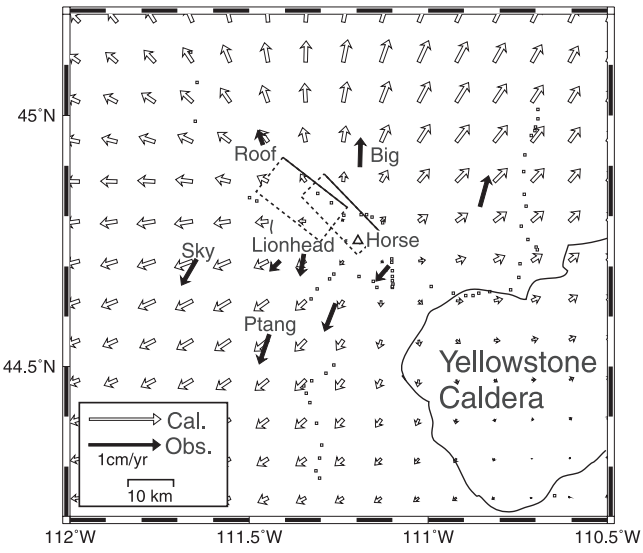

Figure 9. Comparison between the observed and the calculated horizontal velocity during the period of 1973–1987. Solid vectors represent the observed velocities at the trilateration stations with respect to the Horse station indicated by a triangle [*Savage et al.*, 1993]. Open vectors are the synthetic velocities calculated by the best fitting VE-1 model. Names of the selected station are indicated.

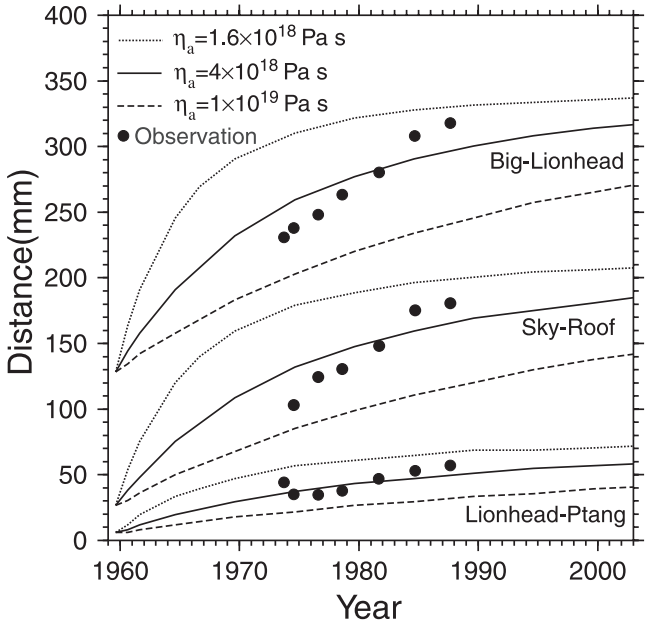

Figure 10. Synthetic postseismic distance change of the 1959 Hebgen Lake earthquake. Solid circles are the observed distance between the stations shown in Figure 8 [*Savage et al.*, 1993]. Curves are calculated for the viscoelastic relaxation with the three different viscosities of the VE-1 model. A constant distance is subtracted from each baseline for convenience in plotting.

each case, the velocities are referenced to trilateration station Horse. The calculated velocity field has a pattern of northeast-southwest extension, which is similar to the observed velocities. However, the observed rate is roughly twice as large as the calculated one. This discrepancy is clearer in Figure 10, which shows observed and computed changes in baseline length versus time for three pairs of trilateration stations. Model curves are shown for three values of half-space viscosity (η_a) which span the range of uncertainty in this parameter. The calculated displacement rates are smaller than observed except for the Lionhead-Ptang baseline. Changes in half-space viscosity from our preferred value (solid curves) cannot improve the fit. The cause of the disagreement is uncertain but may be due to a component of steady state deformation in the observed velocity field.

[26] We note that rate change of the calculated postseismic deformation from 1973 to 1987 is small, indicating the difficulty of identifying transient deformation and distinguishing it from steady state motions. Because the elastic and viscoelastic layers are coupled, the relaxation time of the surface deformation is much larger than the Maxwell time (η/μ) of the medium. The relaxation behavior depends on wavelength of deformation [*Pollitz*, 1997], but Figure 10 illustrates that for $\eta_a \sim 4 \times 10^{18}$ Pa s, which corresponds to a Maxwell time of 2 years, the relaxation time of surface displacement is ~15 years. Transient motions are expected to continue at rates of several millimeters per year for much longer than this nominal 15 years relaxation time.

[27] The present-day deformation field mapped by geodetic measurements may thus comprise both steady state movements and subtle transient effects. Although it is difficult in general to accurately correct for these effects from past earthquakes, we can obtain an estimate of their importance using the rheological parameters obtained here. Figure 11 illustrates this, showing transient velocities computed for three large historic Basin and Range earthquakes. We calculated the present-day (2002) postseismic velocity due to the 1954 Fairview Peak-Dixie Valley earthquake sequence (equivalent M_w7.2) [*Hodgkinson et al.*, 1996], the 1959 Hebgen Lake earthquake (M_w7.3), and the 1983 Borah Peak earthquake (M_w6.9) [*Barrientos et al.*, 1987] using the best fitting VE-1 model. These calculations suggest that the transient horizontal displacement rates near the 1959 Hebgen Lake and 1983 Borah Peak earthquakes are as large as a few millimeters per year, and that about 3 mm/yr of uplift continues in the Hebgen Lake region. Transient motions of somewhat less than a millimeter per year are predicted near the 1954 Dixie Valley-Fairview Peak epicenters. These movement rates are measurable by GPS methods and are large enough to significantly perturb the observed velocity gradients across Basin and Range faults [*Thatcher et al.*, 1999].

4. Conclusion

[28] The postseismic deformation shown by leveling data has been applied to constrain the viscoelastic structure of crust and upper mantle in the epicentral area of the 1959 Hebgen Lake earthquake, northern Basin and Range province. The estimated viscoelastic structure consists of

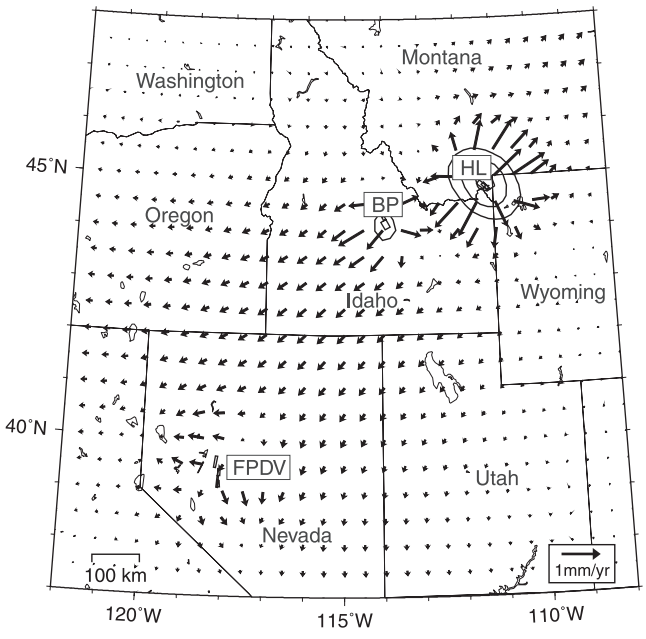

Figure 11. Synthetic postseismic velocity in 2002 due to three historical seismic episodes in the Basin and Range province. Contour line shows vertical uplift rate at the interval of 1 mm. HL, BP, and FPDV denote the 1959 Hebgen Lake earthquake, the 1983 Borah Peak earthquake [*Barrientos et al.*, 1987], and the 1954 Fairview Peak-Dixie Valley earthquake sequence [*Hodgkinson et al.*, 1996], respectively.

an elastic plate whose thickness is 38 ± 8 km and an underlying viscoelastic asthenosphere whose viscosity is $4 \times 10^{18\pm0.5}$ Pa s. The thickness of the elastic plate agrees with that of the crust estimated by the seismological studies. The leveling data do not require relaxation of the lower crust but place a lower bound of 10^{20} Pa s on its effective viscosity.

[29] Estimates of the effective elastic thickness (T_e) of the lithosphere based on the relation between Bouguer gravity and topography are significantly less than the elastic plate thickness found here for the Hegben Lake region. Generally, *Lowry et al.* [2000] found $T_e \sim 5-15$ km in the active western U.S., with estimates of ~10 km in the Hegben Lake area. The reason for this discrepancy is uncertain, but may be related to the different timescales of crustal loading. In our study, the stress unloading due to the 1959 earthquake has been measured over the ~40 years following the earthquake. For the gravity-topography method, T_e represents the thickness of the elastically strong crust that supports loads due to lateral density gradients in the lithosphere, typically isostatically equilibrated over ~1–10 Ma. The difference between the two "elastic" thickness estimates may then be due to stress relaxation of the lower crust for times longer than the observations of postseismic recovery reported here. It is worthwhile noting that the same discrepancy exists in the Lake Bonneville region, where $T_e \sim 8$ km [*Lowry et al.*, 2000] and elastic plate thickness obtained from pluvial lake unloading 12–14 ka B.P. is 25–30 km [*Bills et al.*, 1994; *Nakiboglu and Lambeck*, 1983]. This comparison suggests that if lower crustal relaxation explains the discrepancy this relaxation occurs over times of $\sim10^4-10^7$ years after the lithospheric load is applied.

[30] The observed broad uplift cannot be explained by afterslip on and below the coseismic fault. However, local deformation across the coseismic surface rupture suggests shallow afterslip at the updip extension of the coseismic fault model. This is modeled as 25 cm of normal dip-slip displacement on a rectangular fault 18 km long and 1.7 km wide extending from the surface to 1.2 km depth.

[31] Our results suggest the importance of postseismic viscoelastic relaxation in interpreting the instantaneous deformation field measured with GPS. For example, calculations based on our modeling suggest that the current (2002) postseismic velocities due to the 1959 Hegben Lake and the 1983 Borah Peak earthquakes still exceed 1 mm/yr.

[32] **Acknowledgments.** We thank Dan Dzurisin for providing the leveling data from *Holdahl and Dzurisin* [1991], Jim Savage and Ross Stein for careful review, and Fred Pollitz for useful review and use of his code to calculate the viscoelastic postseismic displacement. Critical reviews by two anonymous reviewers improved the quality of the paper. The coordinates of the Hebgen Lake fault were supplied by M. Machette and R. Dart. We thank Bill Hammond for helpful discussion. We used the GMT3.4 graphic package [*Wessel and Smith*, 1998] to plot most of figures. This study was accomplished while T.N. was a visiting researcher at USGS Menlo Park, funded by the Ministry of Education, Culture, Sports, Science, and Technology (MEXT) of Japan.

References

Barrientos, S. E., R. S. Stein, and S. N. Ward, Comparison of the 1959 Hebgen Lake, Montana and the 1983 Borah Peak, Idaho, earthquakes from geodetic observations, *Bull. Seismol. Soc. Am.*, *77*, 784–808, 1987.

Bills, B. G., and G. M. May, Lake Bonneville: Constraints on lithospheric thickness and upper mantle viscosity from isostatic warping of Boneville, Provo, and Gilbert stage shorelines, *J. Geophys. Res.*, *92*, 11,493–11,508, 1987.

Bills, B. G., D. R. Currey, and G. A. Marshall, Viscosity estimates for the crust and upper mantle from patterns of lacustrine shoreline deformation in the Eastern Great Basin, *J. Geophys. Res.*, *99*, 22,059–22,086, 1994.

Braile, L. W., R. B. Smith, J. Ansorge, M. R. Baker, M. A. Sparlin, C. Prodehl, M. M. Schilly, J. H. Healy, St. Mueller, and K. H. Olsen, The Yellowstone-Snake river plain seismic profiling experiment: Crustal structure of the eastern snake river plain, *J. Geophys. Res.*, *87*, 2597–2609, 1982.

Bürgmann, R., S. Ergintav, P. Segall, E. H. Hearn, S. McClusky, R. E. Reilinger, H. Woith, and J. Zschau, Time-dependent distributed afterslip on and deep below the Izmit earthquake rupture, *Bull. Seismol. Soc. Am.*, *92*, 126–137, 2002.

Chen, W., and P. Molnar, Focal depths of intracontinental and intraplate earthquakes and their implications for the thermal and mechanical properties of the lithosphere, *J. Geophys. Res.*, *88*, 4183–4214, 1983.

Deng, J., M. Gurnis, H. Kanamori, and E. Hauksson, Viscoelastic flow in the lower crust after the 1992 Landers California, earthquake, *Science*, *282*, 1689–1692, 1998.

Dzurisin, D., K. M. Yamashita, and J. K. Kleinman, Mechanisms of crustal uplift and subsidence at the Yellowstone caldera, Wyoming, *Bull. Volcanol.*, *56*, 261–270, 1994.

Hodgkinson, K. M., R. S. Stein, and G. Marshall, Geometry of the 1954 Fairview Peak-Dixie Valley earthquake sequence from a joint inversion of leveling and triangulation data, *J. Geophys. Res.*, *101*, 25,437–25,457, 1996.

Holdahl, S. R., and D. Dzurisin, Time-dependent models of vertical deformation for the Yellowstone-Hebgen Lake region, 1923–1987, *J. Geophys. Res.*, *96*, 2465–2483, 1991.

Iwasaki, T., and M. Matsu'ura, Quasi-static crustal deformations due to a surface load, *J. Phys. Earth*, *30*, 469–508, 1982.

Jackson, J., Strength of the continental lithosphere: Time to abandon the jelly sandwich?, *GSA Today*, *12*, 4–10, 2002.

Kaufmann, G., and F. Amelung, Reservoir-induced deformation and continental rheology in vicinity of Lake Mead, Nevada, *J. Geophys. Res.*, *105*, 16,341–16,358, 2000.

Kohlstedt, D. L., B. Evans, and S. J. Mackwell, Strength of the lithosphere: Constraints imposed by laboratory experiments, *J. Geophys. Res.*, *100*, 17,587–17,602, 1995.

Lambeck, K., C. Smither, and P. Johnston, Sea-level change, glacial rebound and mantle viscosity for northern Europe, *Geophys. J. Int.*, *134*, 102–144, 1998.

Lowry, A. R., N. M. Ribe, and R. B. Smith, Dynamic elevation of the Cordillera, western United States, *J. Geophys. Res.*, *105*, 23,371–23,390, 2000.

Matsu'ura, M., and Y. Hasegawa, A maximum likelihood approach to nonlinear inversion under constraints, *Phys. Earth Planet. Inter.*, *47*, 179–187, 1987.

Milne, G. A., J. L. Davis, J. X. Mitrovica, H.-G. Scherneck, J. M. Johannson, M. Vermeer, and H. Koivula, Space-geodetic constraints on glacial isostatic adjustment in Fennoscandia, *Science*, *291*, 2381–2385, 2001.

Nakiboglu, S. M., and K. Lambeck, A reevaluation of the isostatic rebound of Lake Bonneville, *J. Geophys. Res.*, *88*, 10,439–10,447, 1983.

Nishimura, T., et al., Distribution of seismic coupling on the subducting plate boundary in northeastern Japan inferred from GPS observations, *Tectonophysics*, *323*, 217–238, 2000.

Okada, Y., Surface deformation due to shear and tensile faults in a half-space, *Bull. Seismol. Soc. Am.*, *75*, 1135–1154, 1985.

Peng, X., and E. D. Humphreys, Crustal velocity structure across the eastern Snake River Plain and the Yellowstone swell, *J. Geophys. Res.*, *103*, 7171–7186, 1998.

Pollitz, F. F., Gravitational viscoelastic postseismic relaxation on a layered spherical Earth, *J. Geophys. Res.*, *102*, 17,921–17,941, 1997.

Pollitz, F. F., R. Bürgmann, and P. Segall, Joint estimation of afterslip rate and postseismic relaxation following the 1989 Loma Prieta earthquake, *J. Geophys. Res.*, *103*, 26,975–26,992, 1998.

Pollitz, F. F., G. Peltzer, and R. Bürgmann, Mobility of continental mantle: Evidence from postseismic geodetic observations following the 1992 Landers earthquake, *J. Geophys. Res.*, *105*, 8035–8054, 2000.

Pollitz, F. F., C. Wicks, and W. Thathcer, Mantle flow beneath a continental strike-slip fault: Postseismic deformation after the 1999 Hector Mine earthquake, *Science*, *293*, 1814–1818, 2001.

Reilinger, R., Evidence for postseismic viscoelastic relaxation following the 1959 $M = 7.5$ Hebgen Lake, Montana, earthquake, *J. Geophys. Res.*, *91*, 9488–9494, 1986.

Savage, J., M. Lisowski, W. H. Prescott, and A. M. Pitt, Deformation from 1973 to 1987 in the epicentral area of the 1959 Hebgen Lake, Montana, earthquake ($Ms = 7.5$), *J. Geophys. Res.*, *98*, 2145–2153, 1993.

Smith, R. B., and W. J. Arabasz, Seismicity of the intermountain seismic belt, in *Neotectonics of North America*, vol. 1, *Decade Map*, edited by

D. B. Slemmons et al., pp. 185–227, Geol. Soc. of Am., Boulder, Colo., 1991.

Tabei, T., Crustal movements in the inner zone of southwest Japan associated with stress relaxation after major earthquakes, *J. Phys. Earth*, *37*, 101–131, 1989.

Thatcher, W., T. Matsuda, T. Kato, and J. B. Rundle, Lithospheric loading by the 1896 Riku-u earthquake, northern Japan: Implications for plate flexure and asthenospheric rheology, *J. Geophys. Res.*, *85*, 6429–6435, 1980.

Thatcher, W., G. R. Foulger, B. R. Julian, J. Svarc, E. Quilty, and G. W. Bawden, Present day deformation across the Basin and Range province, western United States, *Science*, *282*, 1714–1718, 1999.

Wessel, P., and W. H. F. Smith, New improved version of generic mapping tools released, *Eos Trans. AGU*, *79*(47), 579, 1998.

Wicks, C., W. Thatcher, and D. Dzurisin, Migration of fluids beneath Yellowstone Caldera inferred from Satellite Radar Interferometry, *Science*, *282*, 458–462, 1998.

T. Nishimura, Geographical Survey Institute, Geography and Crustal Dynamics Research Center, Kitasato-1, Tsukuba, Ibaraki 305-0811, Japan. (t_nisimura@gsi.go.jp)

W. Thatcher, U.S. Geological Survey, 345 Middlefield Road, MS977, Menlo Park, CA 94025, USA. (thatcher@usgs.gov)